ELSEVIER

Sensors and Actuators A 127 (2006) 123–130

A PHYSICAL

www.elsevier.com/locate/sna

Microfabrication of pre-aligned fiber bundle couplers using ultraviolet lithography of SU-8

Ren Yang [a], Steven A. Soper [b], Wanjun Wang [a,*]

[a] *Department of Mechanical Engineering, Center for BioModular Multi-Scale Systems, Louisiana State University, Baton Rouge, LA 70803, United States*
[b] *Department of Chemistry, Center for BioModular Multi-Scale Systems, Louisiana State University, Baton Rouge, LA 70803, United States*

Received 30 July 2005; received in revised form 1 November 2005; accepted 3 November 2005
Available online 20 December 2005

Abstract

This paper describes the design, microfabrication and testing of a pre-aligned array of fiber couplers using direct UV-lithography of SU-8. The fiber coupler array includes an out-of-plane refractive microlens array and two fiberport collimator arrays. With the optical axis of the pixels parallel to the substrate, each pixel of the microlens array can be pre-aligned with the corresponding pixels of the fiberport collimator array as defined by the lithography mask design. This out-of-plane polymer 3D microlens array is pre-aligned with the fiber collimator arrays with no additional adjustment and assembly required, therefore, it helps to dramatically reduce the running cost and improve the alignment quality and coupling efficiency. In addition, the experimental results for the fiber couplers are also presented and analyzed.

Keywords: UV-lithography; Out-of-plane refractive microlens array; Pre-aligned; Fiberport collimator array; Fiber bundle coupler; SU-8; 3D microlens

1. Introduction

Optical fiber is widely used in telecommunication and optical sensors. Fiber couplers are very important components for the optical communication system and fiber optical-based sensors. Fiber couplers are commonly used to manipulate light signal and to complete the connection of light-source-to-fiber, fiber-to-fiber, and fiber-to-detector to relay the optical propagation for illumination delivery or signal collection. By reducing back-reflection and alignment errors, fiber couplers can increase light throughput. The alignment of the optical components in most optical fiber applications is extremely critical for ensuring the maximum amount of light that flows through the coupled devices. Fiber coupling is subject to three types of misalignment: separation (longitudinal misalignment, z-axis), offset (lateral misalignment, x-axis), and tilt (angular misalignment, θ). In longitudinal misalignment, the end of the fibers may not be in the optimized position; if the end of the second optical fiber is positioned away from the image position for the end of the first fiber, light from one fiber core will spread and lose much of its intensity when coupled into the receiving fiber. In the case of offset error, the fiber cores may be displaced laterally along the direction perpendicular with the optical axis; light emitting from one core hits the cladding layer of the second fiber resulting in reduced light throughput. In the third case, one fiber may be tilted (rotated around the x- and z-axis) relative to the other and cause a signal transmission loss.

In a conventional fiber coupler with optical lenses and fibers, the light from the source (such as, laser, diode, lamp, etc.) or the end of another fiber is focused by one or two optical lenses and coupled into another fiber or a detector. In a conventional fiber coupler, a mechanical fiberport collimator is used to precisely adjust the position of the fiber with respect to the lens to obtain the maximum coupling efficiency. Normally, the fiberport collimator needs to be adjustable in several axes, normally x, y, z and θ. The conventional types of mechanical fiberport collimators have a large size and are not easy to be integrated with other optical components. In conventional optical fiber systems, such alignment and assembly are often done manually, therefore increasing the complexity of operation. Also, the cost and the limit of achievable precision in these mechanical fiberports are determined by the complexity of the optical system (i.e., number of couplers and physical dimensions of the fiber) and the operator expertise, respectively.

* Corresponding author. Tel.: +1 225 578 5807; fax: +1 225 578 5924.
E-mail address: wang@lsu.edu (W. Wang).

0924-4247
doi:10.1016/j.sna.2005.11.007

Microfabrication of fiberport and coupling systems is an attractive approach for simplifying the optical system, which incorporate fiber optics. For example, silicon micromachined V-groove fiber couplers [1,2] are attractive and simple devices that can be used to obtain precise alignment of optical fibers and also, can be directly integrated with other optical components. By etching a series of V-grooves on the silicon substrate, high precision coupling of many fibers to other optical devices can be achieved.

There are many methods to fabricate microlenses or microlens arrays and apply them in optical fiber systems. The most commonly used method is to fabricate a spherical tip on the optical fiber to enhance the coupling efficiency to a receiving fiber or other optical component. These ball lenses are fabricated by melting the optical fiber's end to form a lens, which is based on surface tension principles [3]. Micro-jet technology can also be used to place a lenslet at the end of a multimode fiber to improve coupling efficiency [4]. Ball lenses formed by thermal re-flowing of two polymer layers has been shown to be assembled into a silicon-based platform for fiber coupling [5,6].

In this paper, an approach using 3-D UV-lithography of SU-8 photoresist [7,8] is presented for fabricating pre-aligned fiber bundle couplers. This fiber bundle coupler includes a pre-aligned out-of-plane refractive microlens array [9–13] and fiberport collimator arrays. With the optical axis of each pixel parallel to the substrate, each pixel of the out-of-plane microlens array can be pre-aligned with the corresponding pixels of the fiberport collimator arrays in the mask design. The microlens array and fiberport collimator arrays are made using photolithography so that precise alignment can be obtained without accumulation of tolerances. As a simple example of a pre-aligned integrated optical system [11], an out-of-plane polymer microlens array was pre-aligned to fiber collimator arrays in the mask design. In each pixel of the fiber bundle coupler, lateral misalignment and angular misalignment are minimized by this pre-alignment technology. The longitudinal misalignment also can be minimized by the stop function of the fiber-fixing groove in the coupler. As a result, no additional adjustment or assembly was required, leading to dramatically reduced running cost and significantly improved alignment quality and coupling efficiency. This technology for a fiber bundle coupler can also be used to fabricate pre-aligned fiber couplers for just single fiber-to-fiber junctions as well.

In the following sections, the design and working principles for the pre-aligned fiber coupler will be presented followed by the detailed fabrication process used to make the fiber bundle coupler. Finally, some test results for the pre-aligned fiber bundle couplers fabricated with this principle are presented.

2. Design of the fiber bundle coupler and tilted lithography of SU-8

The research work presented in this paper uses a 3-D fabrication method to obtain the pre-aligned fiberport collimator array and out-of-plane polymer microlens array. This technology is based on multiple-step UV-lithography of SU-8 and carefully controlled development process for both the fiberport collimator array and the microlens array. Each pixel of this out-of-plane polymer microlens array is pre-aligned with the corresponding pixels of the fiberport collimator with no additional adjustment and assembly requirement.

When the mask for the optical fiber bundle coupler is designed, the fiberport and the microlens are pre-aligned to the designed position. No changes and adjustment between the mask and the photoresist on the substrate are needed during the lithography process. The precision of the pre-assembled fiber bundle coupler is therefore limited by the optical mask used. Without any assembly and alignment, this microlens' optical axis is parallel to the substrate on which the whole optical system is built. This unique advantage makes it possible to design and fabricate pre-aligned fiber bundle couplers with precise alignment and high coupling efficiency.

The fabrication and working principle for the fiber bundle coupler are shown in Fig. 1. Because SU-8 is a negative tone photoresist, the exposed regions remain after lithography and development. The entire fiber bundle coupler is designed on a single photomask. Two exposures at $\pm 45^\circ$ tilt angles with respect to the surface normal are conducted for the out-of-plane microlens array fabrication. When two cylindrical light beams in perpendicular are projected on the SU-8 resist, two perpendicular cylindrical structures are formed at $\pm 45^\circ$ angles with respect to the substrate and the intersected region of the resist is double-exposed. This faceted surface of the intersected region includes four pieces of cylindrical surfaces. The lithography light used is an *h*-line ($\lambda = 405$ nm) dominated UV light source with optimized dosage and wavelength selection ratio. The position between the substrate and the mask are fixed during and after the exposure for the microlens and microlens array. With a defined region of the microlens or microlens array covered using a shade mask, the fiberport collimator array is then fabricated lithographically using an *i*-line ($\lambda = 365$ nm) dominated broadband UV light source in an optimized exposure dosage and wavelength selection ratio.

The development rates for the unexposed SU-8 and exposed SU-8 with different exposure dosages are different. By careful control of the exposure dosages, wavelength selection, and the optimized development time, the intersection regions are developed into the out-of-plane microlens and microlens array [9–13]. The rectangle posts tilted at $\pm 45^\circ$ formed the fiberport collimator. The final shape of this fiber bundle coupler after development is schematically shown in Fig. 1(C). In a practical lithography process, each pixel of this convex microlens array can be expected to have a quasi-spherical shape with a smooth surface profile and its optical axis is overlapped with the central line of the square opening for the corresponding fiberport collimator. Each pixel of the out-of-plane microlens can be aligned with the corresponding pixel of the fiberport collimator as schematically shown in Fig. 1(D). A single optical mask used therefore determines the pre-alignment precision of the whole fiber coupler.

To obtain a cylindrical light beam in a tilted exposure of SU-8 at $\pm 45^\circ$ for the out-of-plane microlens and microlens array fabrication, the opening in the photomask must be of a conic shape. The conic curves associated with various values of the conic

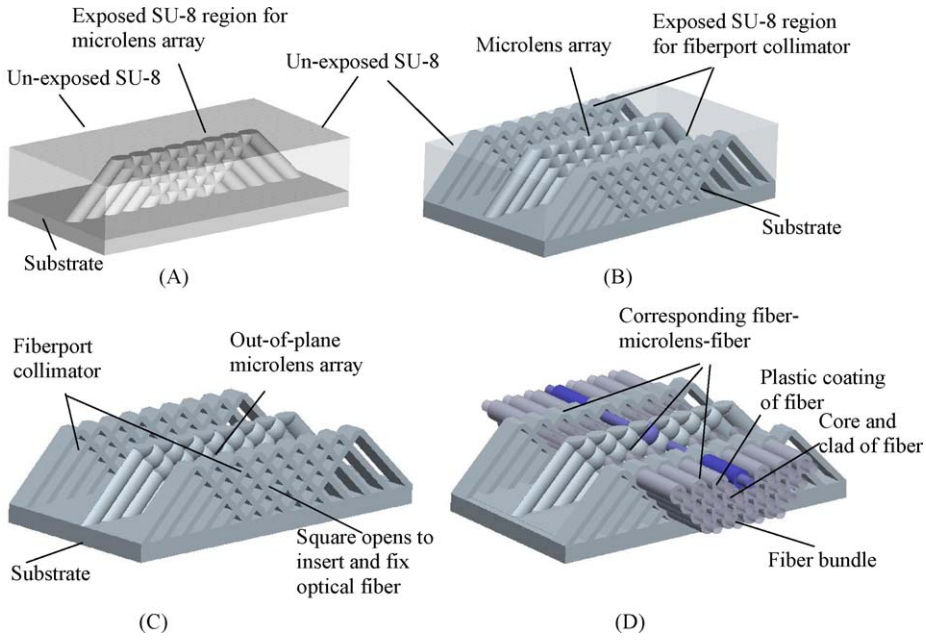

Fig. 1. Fiber bundle couplers. (A) ±45° tilted expose for the out-of-plane microlens array region. (B) Covering the microlens array region by a shade mask with a ±45° tilted expose for the fiberport collimator region with the same mask. (C) After development, each pixel of the microlens array and corresponding pixel of the fiberport collimator array are precisely aligned. (D) Diagram showing the position of the fibers after inserting the fiber bundle, in which the corresponding fiber–microlens–fiber system are marked in blue for clear definition of the optical path.

constant can be used for the mask pattern of the out-of-plane microlens or microlens array, depending on the requirements for the microlens' surface profile. The ellipse, circle, parabola, and hyperbola can be used for the mask pattern for the out-of-plane microlens or microlens array to achieve the corresponding surface profiles. In general, the curvature of the mask opening along the designed optical axis control the surface profile and curvature of the microlens along the same optical axis. However, since the development rate also plays significant rule in the process, the mechanism is very complicated [11]. After stripping the plastic coating layers, the diameter of the center glass fiber (include core and clad) used here is 125 μm. Because of the 45° tilted lithography, the distance between the two open blocks for the fiberport collimator, as shown in Fig. 2, is $125\sqrt{2}$ μm to obtain a square opening with dimensions of 125 μm by 125 μm to fix the optical fiber. If the fiber's diameter of the core and clad changes, corresponding changes in the designed dimensions of the fiberport collimators need to be made. For easy development of the square channels for the fiberport collimators, the long square holes are separated by several cascaded pieces as shown in Fig. 2. In order to insert the optical fibers into the fiberport collimators easily, an opening larger than the optical fibers' outside diameter can be designed as shown in Fig. 2.

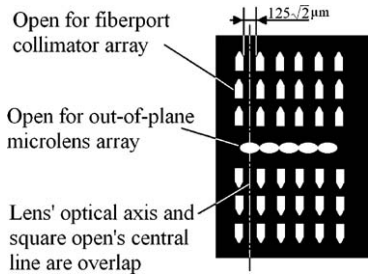

Fig. 2. Mask patterns for the fiber bundle coupler.

3. Fabrication of the fiber bundle coupler

3.1. Wavelength selection and refraction compensation in tilted lithography

The lithography light used for the out-of-plane microlens and microlens array fabrication is an *h*-line (λ = 405 nm) dominated broadband UV light with optimized dosage and wavelength selections light (in Fig. 3, marked as "light intensity after PMMA filter"). The transmission of a 1 mm thick unexposed SU-8 100 is

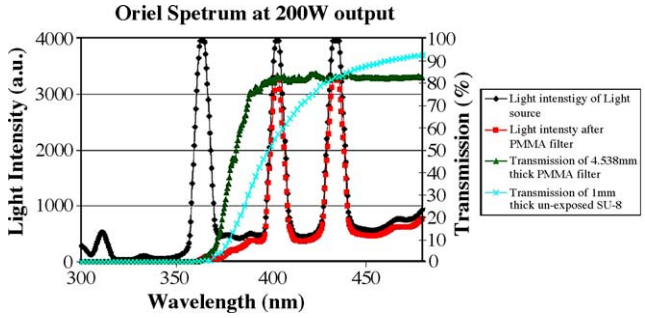

Fig. 3. Measured transmission spectrum of a 1 mm thick unexposed SU-8 100 resist, transmission spectrum of the PMMA filter, and the light intensity of the UV station with and without the PMMA filter. The data was obtained using Ocean Optics' S2000 spectrometer and coupling fiber, the receiving end of the fiber was oriented in parallel with the light beam of the Oriel UV station.

measured as shown in Fig. 3. The components of shorter wavelengths are primarily absorbed in the surface region while the longer wavelength components penetrate further down into the resist and expose the bottom region. The absorption coefficient of unexposed SU-8 for the *h*-line (λ = 405 nm) is about one fourth that of the *i*-line (λ = 365 nm), and three times that of the *g*-line (λ = 436 nm). In order to improve the exposure uniformity for the entire area of the microlens array, wavelengths shorter than 365 nm needs to be filtered to avoid over-exposure of the surface layer. Longer wavelengths (either *g*-line or *h*-line) with much lower absorbances are used to permit more energy to reach the bottom part of the thick SU-8 resist layer and to achieve better uniformity of the absorbance. In our experiment, a 4.54 mm thick PMMA sheet was used as a filter and an Oriel UV station was used for the lithography. The transmission of this PMMA sheet is about 0.3% at the *i*-line, 82% at the *h*-line, and 82% at the *g*-line. The light intensities of the Oriel UV station with 200 W output before and after the PMMA filter and the transmission of the PMMA filter are also shown in Fig. 3.

Because the absorbance at the *h*-line is about three times that of the *g*-line, the lithography process for the out-of-plane microlens and microlens array region is *h*-line dominated. During the development process, not only the unexposed SU-8 is removed, the exposed regions may also be dissolved during development, although at a much lower rate. The development rate for the unexposed SU-8, single-exposed SU-8, and double-exposed SU-8 also occur at different rates. During the development process, the single-exposed region is dissolved at a much higher rate than that of the double-exposed region. The unexposed SU-8 is normally developed many times faster than the exposed SU-8. Our previously reported work [9–13] proved that these intersection areas form microlenses with quasi-spherical surface profiles. In addition to the mask pattern geometry, surface profiles of the microlenses are also affected by exposure dosage, wavelength selection, development conditions, and bake conditions.

Sato et al. also reported an interesting work on multi-angle tilted lithography of SU-8 [14]. In their work, the surface profile control is not important and the focus was on making through holes for fluidic filter application. The light source used for the lithographic fabrication of the fiberport collimator array is the *i*-line (λ = 365 nm) dominated broadband UV light as marked as "light intensity of light source" in Fig. 3. Full exposure dosage was used for the fabrication of the fiberport collimators to make sure the bottom part of the device receives sufficient exposure dosage and is fully cured. The dissolving rate of these sections of the exposed SU-8 in the development process is negligible and the shape of the fiberport collimator array can therefore be assumed to depend only on the geometry of the mask pattern.

The refraction of the light at the surface of the SU-8 resist is dependent on the wavelengths of the light source. For the *h*-line light (λ = 405 nm), the refractive index, *n*, is 1.650, the critical angle is 37.305°. For the *i*-line light (λ = 365 nm) with *n* = 1.660, the critical angle is 36.836°. To obtain 45° exposure angles inside the SU-8 resist, a coupling prism and optical liquid glycerin (glyceryl) were required to compensate for refraction at these interfaces [9–11] as schematically demonstrated in Fig. 4.

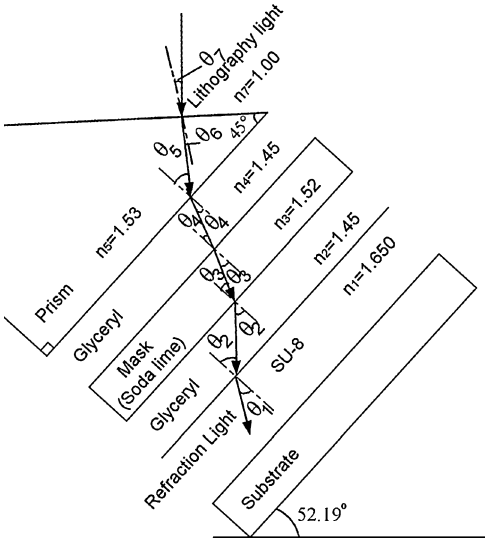

Fig. 4. Refraction compensation principle to obtain 45° refractive angle at λ = 405 nm. To provide refraction compensation when λ = 365 nm, just change the angle of 52.19 to 53.32°.

3.2. Microfabrication of pre-aligned fiber bundle coupler

The fabrication procedure for the pre-aligned fiber coupler using direct lithography is as follows: (1) conduct tilted exposures for the microlens and microlens array; (2) with the position between the substrate and the mask fixed and a shade mask to cover the pattern for the microlens or microlens array, use a tilted exposure for the fiber-fixing grooves with full exposure dosages and different wavelengths; (3) develop the sample.

A layer of 1100 μm thick SU-8 100 was spin-coated onto a silicon substrate at 400 rpm for 20 s. The sample was then soft-baked at 110 °C for 10 h and ramped down to room temperature in 8 h. Two consecutive exposures were done in the fabrication process while the optical mask and the wafer were held mechanically without any adjustment. In the first exposure, the sample was tilt-exposed at ±45° to fabricate the microlens or microlens array. In this exposure, the exposure dosage and light source wavelength were carefully controlled to obtain the desired lens profile [9–11]. After the exposure for the microlens or microlens array, a shadow mask was placed on the optical mask to cover the regions containing the microlens array. The second tilted-exposure at ±45° was conducted to fabricate the fiber-fixing grooves using a full exposure dosage. The sample was then post-baked at 96 °C for 20 min and cooled down to room temperature in no more than 12 h. After the unexposed regions were removed in development stage, the remaining exposed regions of resist formed the microlens array and fiber-fixing grooves.

Three types of mask openings are used here: ellipse with long axis $\sqrt{2}$ times of the short axis and the long axis perpendicular to the lens' optical axis (Group 1); circular openings for ball lens (Group 2); and ellipse with long axis aligned to the lens' optical axis and equal to $\sqrt{2}$ times the short axis (Group 3). Fig. 5 shows a SEM Image of a prototype fiber bundle holders (Group

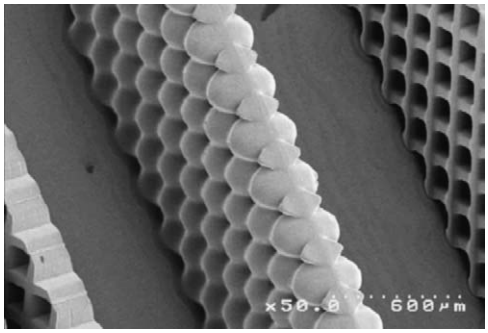

Fig. 5. SEM image of a prototype fiber bundle holder (Group 3) fabricated using an elliptical mask pattern with long axis aligned to the lens' optical axis: $250\sqrt{2}$ μm (*L*), 250 μm (*S*).

3) fabricated using the direct lithography method as presented in this paper.

After obtaining the SU-8 microstructures for the out-of-plane microlens and fiber holder-grooves, optical fibers were inserted into the fiber grooves to complete the construction of the fiber couplers for our optical tests. The optical fiber were prepared by stripping the plastic cladding from the fiber and then cut to a required length so that it can be inserted into the groove holder of the coupler. When the fiber was inserted into the coupler, it was held in place by these grooves. The length of the stripped fiber determines the separation between the terminal of optical fiber and the surface of microlens.

The ends of the optical fibers were stripped of their plastic coating by fiber stripping tools and fiber end terminated using a fiber cleaver (Thorlabs Inc., Newton, NJ). The terminated optical fibers are then inserted into the holding grooves of the fiber coupler. Fig. 6(A)–(C) shows several SEM images of the fabricated fiber coupler with only one optical fiber inserted into the array. From the SEM images, it can be seen that each pixel of the microlens is pre-aligned with its corresponding fiber holders.

4. Experimental results and discussions

A simple test was conducted to test the focusing capabilities of the microlens array. A collimated red light beam (about 630 nm) was projected onto the backside of the out-of-plane microlens array and the focused image was acquired using CCD camera (DXC-960MD SONY) in a Nickon OPTIPHOT-88 optical measurement microscope. Fig. 7 shows a photograph of the focused image. The pixels at the array's edge are partial microlens so the focal pads are not as bright as the pixels contained within the central region of the array. The pixel size of

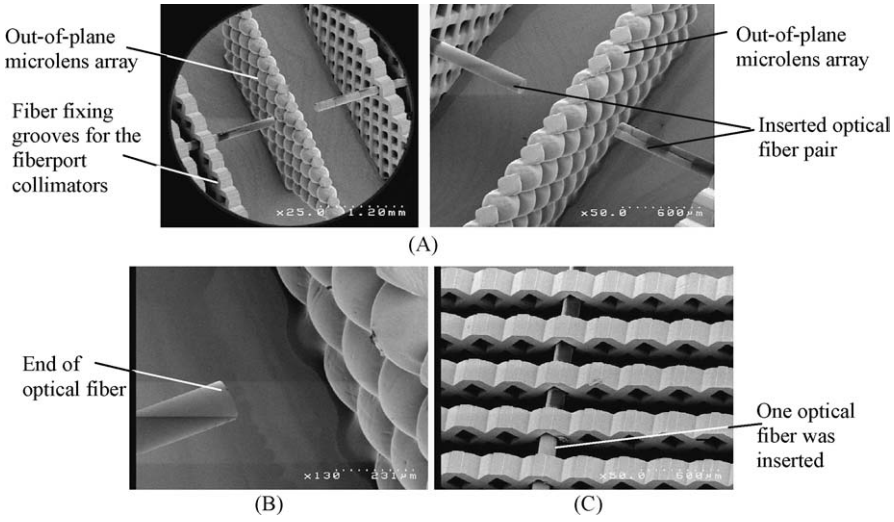

Fig. 6. SEM image for the fiber coupler: (A) fiber coupler; (B) surface profile of the out-of-plane microlens array; (C) cascaded fixing grooves of the fiberport collimator.

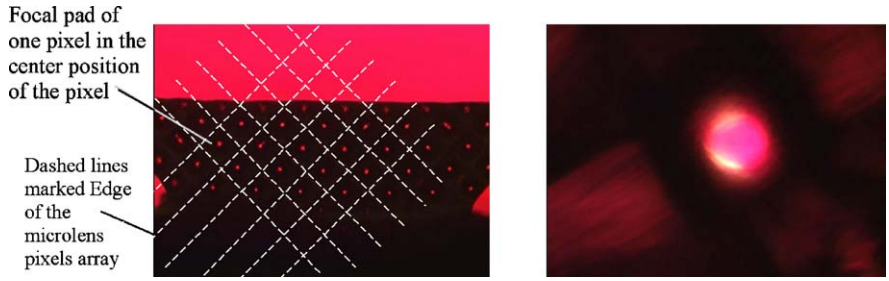

Fig. 7. Optical images of the focal pads of the out-of-plane microlens array with collimated red light projected on the backside. The dashed white lines are used for visualization to help locate the individual pixels of the array. The picture at the right is a zoomed image of the focal pad.

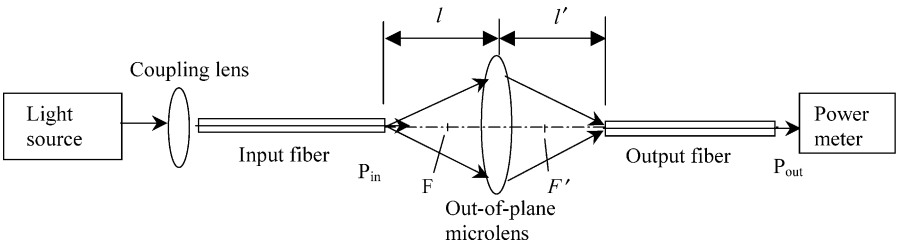

Fig. 8. Schematic diagram of the experimental setup for determining the coupling efficiency of the fiber bundle coupler.

the microlens array shown in the photograph was 247.89 μm by 247.89 μm. The size of the focused pads can be estimated to have a diameter of 18.72 μm.

The experimental setup for determining the optical system's coupling efficiency is schematically shown in Fig. 8. A broadband light source (A1010 Arc lamp, Photon Technology International) or laser diode (DL5038-021, Thorlabs, Nowton, NJ) served as the light source, which was then focused using a coupling microscope objective lens (NA = 0.4, 40×). The plastic coating at the end of an optical fiber was stripped and then terminated using a cleaver. One end of the fiber was then fixed on the fiberport collimator facing the microscope objective lens. The fiberport collimator's relative position was then adjusted with respect to the microscope lens to obtain maximum output power at the opposite end of the fiber. A power meter (FieldMate 1067353, Coherent Inc., Santa Clara, CA) was used to measure the input/output light power. In each measurement, the end of the output fiber is perpendicular with the photo-cell and slightly touching on the central area of the cell surface. This helped to reduce the measurement error and improved the repeatability of focus/align. After the output power from the first optical fiber was measured, it was then inserted into one of the holder-grooves in the fiberport collimator with the help of a microscope. The second optical fiber (the receiving fiber) was inserted into the holder-groove on the opposite side. The output power, P_{out}, for the receiving optical fiber was then measured to obtain the coupling efficiency, P_{out}/P_{in} ($dB = -10\log(P_{out}/P_{in})$).

The distances between the fiber pair and the coupling microlens can be adjusted to obtain the highest coupling coefficient. Fig. 9 shows a photo image of the prototype fiber bundle coupler with one pair of fibers inserted into the coupler and light supplied. The distances between the microlens array and the ends of the fibers, l and l', are close to two times the focal length (f) with l slightly longer than $2f$ and l' slightly shorter than $2f$. If the numerical aperture (NA) of the microlens and the optical fiber are matched (i.e., microlens' NA equals or larger than optical fiber's NA), the highest coupling efficiency ($dB = -10\log(P_{out}/P_{in})$) can be achieved. In addition, the cross-talk between neighboring channels was also tested by measuring the output powers of several different receiving fibers not positioned directly within the optical train and compared with the input light power.

Both multi-mode optical fibers (GIF625 from Thorlabs Inc., Newton, NJ) and single mode fibers (TBII single mode fiber, Corning Inc., Corning, NY) were used in our tests for the fiber coupling efficiency. The GIF625 fiber is a graded index fiber with NA = 0.275 and a core diameter of 62.5 μm. The TBII single mode fiber has a NA of 0.13 and core diameter of 8 μm. Both a broadband light source and a 635 nm laser were used in these tests. For the multi-mode optical fiber, the coupling efficiency was measured to be 44.7% using the broadband light source, and 24.5% using a laser diode with a wavelength of 635 nm. For the single mode optical fiber, the coupling efficiency was found to be about 22.7% for the laser diode at 635 nm. Because the prototype lens has some significant aberration, this may have made the focus pad for broadband light sources better at some position, therefore higher coupling efficiency.

All three groups of out-of-plane microlens arrays with different surface profiles and dimensions were tested. The total coupling efficiency with the 635 nm laser is shown in Fig. 10. For all of these fiber couplers, the cross-talk between neighboring fiber pairs was also measured and the amount of light leaking into these fibers was too small to be measured by our power meter, therefore indicating that the degree of cross-talk was minimal.

In the coupling efficiency test, the light reflection and the absorption by the structural material, cured SU-8 polymer, also needs to be considered. Partial reflection exists at the interfaces between materials of different refractive index (such as air and glass, cured SU-8). The percentage of the reflection at a particular interface depends upon the refractive indices, angle of

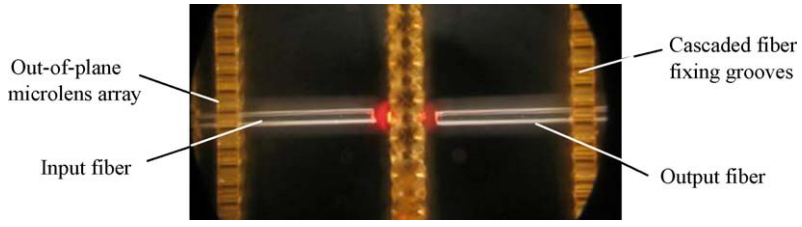

Fig. 9. Photograph of the top view of the fiber bundle coupler with one pair of fibers inserted into the coupler and the light from a laser diode (λ = 635 nm) supplied to the fiber pair.

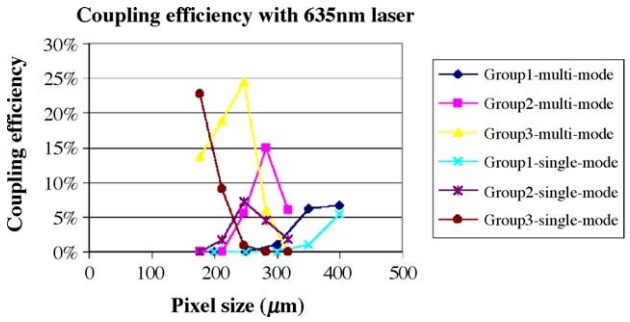

Fig. 10. Coupling efficiency for the fiber coupler with different surface profiles and dimensions.

incidence and the polarization state of the light. In the case of normal incidence, the following equation is used to estimate the back-reflection:

$$\mathrm{BR} = \frac{(n_2 - n_1)^2}{(n_2 + n_1)^2} \tag{1}$$

At normal (0°) incidence, light transiting between air and another optical material with an index of 1.496 (fused silica at 632.8 nm) will suffer an insertion loss of 0.15 dB or 3.3% of the incident light is reflected. At normal (0°) incidence, light transiting between air and material with an index of 1.596 (cured SU-8 at 632.8 nm) will have an insertion loss of 0.24 dB or 5.3% of the incident light is reflected. These reflections result in a reduction in the coupling efficiency of the fiber-to-fiber coupler. To calculate the coupling efficiency for the fiber bundle coupler, reflections at a total of five interfacial surfaces need to be accounted for: one terminal of the input optical fiber, two lens' surfaces, and two terminal faces of the output optical fiber. The total insertion loss can be calculated as:

$$1 - (1 - 0.033)^3 \times (1 - 0.053)^2 = 18.9\%. \tag{2}$$

The attenuation of the SU-8 microlens is estimated to be about 5%. The theoretical coupling efficiency (assuming losses only induced by reflection and SU-8 attenuation) that could be achieved is ~76.1% for the fiber–microlens–fiber coupler system presented in this work. However, the experimentally obtained coupling efficiency for this system was found to be 25% for the multi-mode fiber and 23% for the single-mode fiber as shown in Fig. 10, which are much lower than the theoretical value of 76.1%.

There may be three reasons for the lower than expected coupling efficiency: (1) the relative position between the optical mask and the photoresist changed during lithography; (2) the optical aberration caused the focal pads of the microlenses to become larger than the end size of the fiber core; (3) the numerical aperture numbers between the fiber and the microlens were not matched; (4) errors caused by the fiber inserted into the holder.

In the foregoing estimation of coupling efficiency, it was assumed that no positional changes occurred between the mask and the photoresist on the substrate during the UV-lithography of SU-8. However, glycerin liquid was filled between the resist on the sample wafer and the optical mask to minimize the diffraction caused by the significant air gap between the resist and mask. Glycerin is also necessary for the reflection composition for 45° tilt exposure. A simple mechanical clip was used to hold the wafer and the mask during the tilted exposures (at ±45°). The glycerin liquid layer reduces the friction between the mask and the photoresist, but increased the possible sliding movement. Positional shift between the mask and the photoresist on the substrate may reach several or even tens of microns. This shift caused errors in the subsequent multiple exposures and significantly reduced the fabrication precision and the alignment precision for the fiber coupler. The alignment error therefore contributed to the reduced coupling efficiency. A better design for the mechanical holder is therefore necessary to improve the lithography quality. The holder should permit rotation for well-controlled angles for the tilted lithography and maintain precise position control during lithography to avoid possible positional shift.

The diameter of the focal pads is determined by the surface profile of the microlens. The defects on the lens surface and the surface roughness may also affect the quality of the focal pads. In future work, the lithography conditions such as the mask pattern shape, exposure dosage, wavelength selection, development conditions, and bake conditions, need to be further studied to obtain the optimal process parameters for better surface profile and surface quality. In addition, optical aberration of the microlenses can be reduced by better control for the surface profile as further understanding for the relationship between development rate and lens profile is achieved in the future.

The prototype fiber coupler presented in this paper used only one microlens for one fiber-lens-fiber channel. Using a single microlens in coupling may cause mismatch in the numerical aperture (NA) between the fiber and the microlens. Two cascaded microlenses with each lens symmetrically mirrored another lens for the fiber coupler, one for the input fiber and another for the output fiber, may help to improve the NA match and reduce possible longitudinal misalignment. In addition, this symmetrical structure will help to reduce the optical aberration for the lens pair. Further improvement may also be achieved by reducing the distances between the fiber holders and the focusing lens to avoid misalignment caused by mechanical deflection of fiber that is basically a cantilever. In addition, variations in the lengths of the stripped fiber might also affected the longitudinal alignment accuracy and contributed to the signal loss.

5. Conclusions

We have presented the design, microfabrication and test of pre-aligned array of fiber couplers using direct UV-lithography of SU-8. Each unit in the fiber coupler array consists of an out-of-plane refractive microlens and two fiberport collimators. With the optical axis of pixels parallel with the substrate, each pixel of the microlens array was found to be pre-aligned with the corresponding pixels of fiberport collimator arrays in lithography mask design. No additional adjustment and assembly are therefore required for the integrated fiber coupler array. This helps to reduce the running cost and improve the alignment quality

and coupling efficiency. The experimental results have proved the feasibility of the integrated design approach and fabrication using a single optical mask with direct UV-lithography of SU-8. The coupling efficiency was found to be 25% for multi-mode fiber and 23% single-mode fiber, much lower than the theoretical maximum value of 76.1%. Further improvement may be made using better mechanical holder in lithography to prevent sliding errors and using two focusing lenses with symmetrically mirrored structure.

Acknowledgements

The research work presented was partially funded by Louisiana Space Consortium and the NIH (EB002115). The authors also gratefully acknowledge the financial support of this work through the National Science Foundation (DBI-0138048; EPS-0346411) and partial support through the Louisiana Board of Regents. The authors would like to thank Jason Emory for his help in preparing the optical instruments for coupling efficiency test.

References

[1] K. Song, J. Bu, Y. Jeon, C. Park, J. Jeong, H. Koh, M. Choi, Micromachined silicon optical bench for the low cost optical module, Proc. SPIE Int. Soc. Opt. Eng. 3878 (1999) 375–383.
[2] H. Han, J.D. Stack, J. Mathews, C.S. Koehler, E. Johnson, A.D. Kathman, Integration of silicon bench with micro optics, Proc. SPIE Int. Soc. Opt. Eng. 3631 (1999) 234–243.
[3] T. Abe, Z. Ito, M. Enomoto, Y. Matsumura, New Fabrication Technique of Lens-ended Fibers for Optical Connector, No. 6, vol. 1, Tohoku Kogyo Daigaku Kiyo, Rikogakuhen, 1986, pp. 21–27.
[4] W.R. Cox, T. Chen, D. Ussery, D.J. Hayes, J.A. Tatum, D.L. MacFarlane, Microjetted lenslet triplet fibers, Opt. Commun. 123 (4-6) (1996) 492–496.
[5] H. Yang, C. Chao, C. Lin, S. Shen, Micro-ball lens array modeling and fabrication using thermal reflow in two polymer layers, J. Micromech. Microeng. 14 (2) (2004) 277–282.
[6] C.T. Pan, Silicon-based coupling platform for optical fiber switching in free space, J. Micromech. Microeng. 14 (1) (2004) 129–137.
[7] R. Yang, J.D. Williams, W. Wang, A rapid micro-mixer/reactor based on arrays of spatially impinging micro-jets, J. Micromech. Microeng. 14 (10) (2004) 1345L 1351.
[8] R. Yang, D.L. Feeback, W. Wang, Microfabrication and test of three-dimensional polymer hydro-focusing unit for flow cytometry applications, Sens. Actuators A: Phys. 118 (2) (2005) 259–267.
[9] R. Yang, W. Wang, Fabrication of out-of-plane SU-8 refractive microlens using directly lithography method, in: Proceedings of the SPIE: SPIE Photonics West, vol. 5346, San Jose, CA, 2004, pp. 151–159.
[10] R. Yang, W. Wang, Out-of-plane polymer refractive microlens fabricated based on direct lithography of SU-8, Sens. Actuators A: Phys. 113 (1) (2004) 71–77.
[11] R. Yang, W. Wang, Numerical and experimental study on an out-of-plane pre-aligned refractive microlens fabricated using UV lithography method, Opt. Eng. 43 (12) (2004) 3096–3103.
[12] R. Yang, S.A. Soper, W. Wang, Fabrication of out-of-plane concave and convex refractive microlens array, in: Proceedings of the SPIE: SPIE Photonics West, vol. 5717, San Jose, CA, 2005, pp. 134–141.
[13] R. Yang, W. Wang, S.A. Soper, Out-of-plane microlens array fabricated using ultraviolet-lithography, Appl. Phys. Lett. 86 (2005) 161110.
[14] H. Sato, T. Kakinuma, J.S. Go, S. Shoji, A novel fabrication of in-channel 3-D micromesh structure using maskless multi-angle: exposure and its microfilter application, in: Proceedings of the IEEE MEMS Conference, Kyoto, Japan, 2003, pp. 223–226.

Biographies

Ren Yang received his BS degree in Precision Instruments in May 1996 and his MS degree in optical engineering in March 1999, both from Tsinghua University of China. From June 1999 to August 2001, he studied microelectromechanical systems (MEMS) in Louisiana State University and received MS degree in Engineering Science in May 2002. From September 2001 to February 2003, he worked in Ball Semiconductor Inc. in Dallas, Texas, as an optical engineer. Since March 2003, he works with the Department of Mechanical Engineering in Louisiana State University as a research associate.

Steven A. Soper received his BS degree in Psychology in 1980 and his BS degree in Chemistry in Chemistry in 1982, both from University of Nebraska. He obtained his PhD in Chemistry in 1989 from University of Kansas and worked as postdoc in Los Alamos National Laboratory from 1989 to 1991. He joined the faculty of LSU Chemistry Department in 1991 and currently is the William L. & Patricia Senn, Jr. Professor of Chemistry, Louisiana State University.

Wanjun Wang received his BS in Mechanical engineering from Xian Jiaotong University of China in December 1981. He received his MS and PhD degrees from The University of Texas at Austin in 1986 and 1989, respectively. He joined the faculty of Mechanical Engineering of Louisiana State University in 1993. His current research interests include MEMS technologies, sensors and actuators.